

Synthesis, Modeling, and RET Protein Kinase Inhibitory Activity of 3- and 4-Substituted β -Carbolin-1-ones

Raffaella Cincinelli,[§] Giuliana Cassinelli,[¶] Sabrina Dallavalle,^{*,§} Cinzia Lanzi,^{*,¶} Lucio Merlini,[§] Maurizio Botta,^{*,#} Tiziano Tuccinardi,[†] Adriano Martinelli,[†] Sergio Penco,[§] and Franco Zunino[¶]

Dipartimento di Scienze Molecolari Agroalimentari, Università di Milano, Via Celoria 2, 20133 Milano, Italy, Unità di Chemioterapia e Farmacologia Antitumorale Preclinica, Dipartimento di Oncologia Sperimentale e Laboratori, Fondazione IRCCS Istituto Nazionale dei Tumori, Via Venezian 1, 20133 Milano, Italy, Dipartimento Farmaco Chimico Tecnologico, Università degli Studi di Siena, Via De Gasperi 2, 53100 Siena, Italy, and Dipartimento di Scienze Farmaceutiche, Università di Pisa, Via Bonanno 6, 56126 Pisa, Italy

Received June 27, 2008

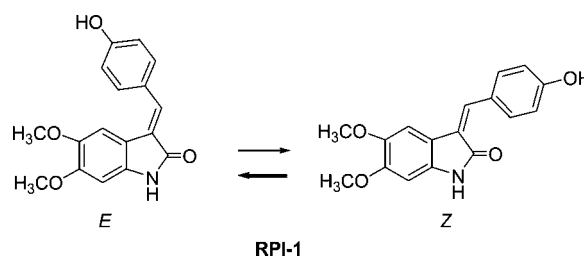
A series of β -carbolin-2-ones and 3,10-dihydro-2*H*-azepino[3,4-*b*]indol-1-ones have been designed, synthesized, and evaluated as RET protein kinase inhibitors on the basis of their structural similarity with the prototype indolin-2-one RPI-1. Some β -carbolin-2-ones (structure 2) showed an ability to inhibit RET enzymatic activity in vitro and proliferation of RETC634R oncogene-transformed NIH3T3 cells comparable to that of the reference compound. The docking analysis of the interaction of these compounds with the crystallographic structure of RET tyrosine kinase domain suggested a new binding interaction scheme different from the one proposed during their design. The rigid structure of the compounds of this series represents a new scaffold with potential advantages in the design of RET protein kinase inhibitors.

Introduction

Gain-of-function mutations of the RET gene have been implicated as driving oncogenic alterations in thyroid cancer.^{1,2} RET encodes the receptor tyrosine kinase for glial cell line-derived neurotrophic family factors. Chromosomal rearrangements known as RET/PTCs are specifically detected in a subset of papillary thyroid carcinomas, whereas missense point mutations are associated with the medullary variant (MTC^a) occurring either sporadically or in a familial pattern.³ In particular, somatic mutations of RET are found in sporadic cases and germline mutations have been identified as the cause of multiple endocrine neoplasia type 2 (MEN 2) inherited cancer syndromes which include MTC as a main component of the disease. Both germline and somatic RET mutations produce dominant-acting oncogenic proteins endowed with constitutive tyrosine kinase activity.¹

Activated oncogenes involved in tumor pathogenesis are attractive targets for new selective therapies.⁴ The potential role of RET oncogenes and their products as targets for thyroid cancer therapy has been supported by several preclinical studies using both gene therapy and pharmacological approaches.^{5,6} In such studies, the inhibition of RET activity has been shown to cause in vitro reversion of the cell transformed phenotype and to produce an antitumor effect against in vivo human MTC xenografts. The occurrence of tumor regressions associated with apoptosis and reduced angiogenesis in animals treated with anti-Ret targeted therapy has also been documented.^{7–9} These effects

Chart 1. Configurational Equilibrium of RPI-1



are indeed consistent with the concept of “oncogene addiction” whereby RET oncogene-harboring thyroid cancers may depend on RET oncogenic pathways for their sustained proliferation and survival.¹⁰ RET targeting thus appears to be a promising approach for the treatment of specific thyroid cancers, although a clinically useful option is still not available.

Among the different strategies developed to abrogate RET oncogenic activity, the use of small molecule inhibitors is currently the most suitable for clinical testing. Several tyrosine kinase inhibitors have been reported to inhibit RET activity including natural¹¹ and synthetic compounds belonging to different structural classes.^{5,6} A few of these compounds, all characterized by multikinase inhibitory activity, have recently entered phase II clinical trials, such as the anilinoquinazoline ZD6474 (vandetanib), the nicotinamide AMG706 (motesanib), the bis-aryleurea BAY43-9006 (sorafenib), and the indolinone SU11248 (sunitinib).^{12–14}

The indolinone-based structure represents a useful scaffold for the design of tyrosine kinase inhibitors.¹⁵ We previously reported the in vitro and in vivo activity profile of the indolin-2-one compound RPI-1 (formerly Cpd1),^{7,9,16,17} an orally available inhibitor of the RET and MET tyrosine kinases.¹⁸

Similar to other indolin-2-ones,¹⁹ it undergoes configurational equilibrium. In polar solvents the RPI-1 *E* configuration (Chart 1) is favored. However, in a recent modeling study of the RET TK binding domain,²⁰ RPI-1 interacted with the model only in the *Z* configuration. This finding is consistent with crystallographic studies showing that other indolin-2-ones bind to ATP

* To whom correspondence should be addressed. For S.D.: phone, +39(0)250316818; fax, +39(0)250316801; e-mail, sabrina.dallavalle@unimi.it. For C.L.: phone, +39(0)223902627; fax, +39(0)223902692; e-mail: cinzia.lanzi@istitutotumori.mi.it. For M.B.: phone, +39(0)577234306; fax, +39(0)577234333; e-mail, botta@unisi.it.

[§] Università di Milano.

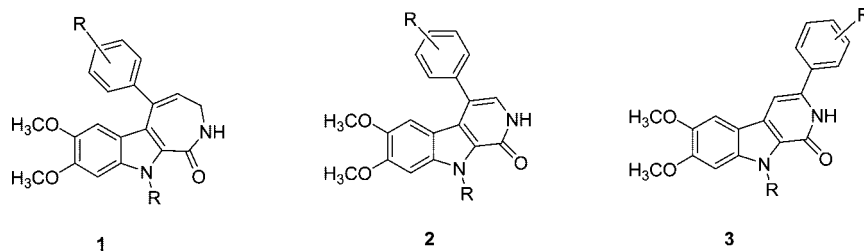
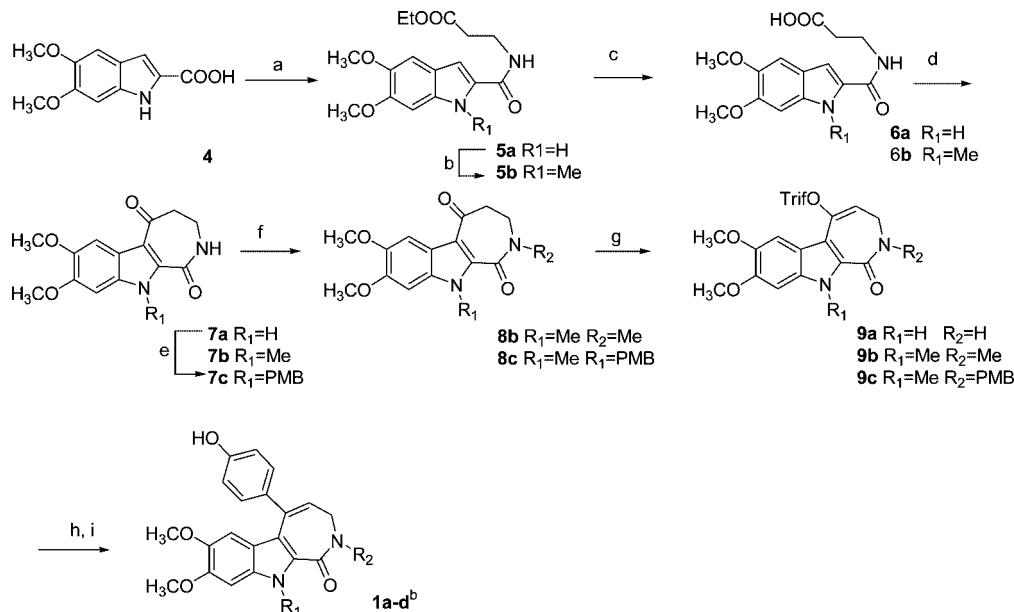
[¶] Istituto Nazionale dei Tumori.

[#] Università di Siena.

[†] Università di Pisa.

^a Abbreviations: MTC, medullary variant carcinoma; MEN 2, multiple endocrine neoplasia type 2; rmsd, root-mean-square deviation; MD, molecular dynamics; MM-GBSA, molecular mechanics generalized Born surface area; MBP, myelin basic protein; CG, conjugate gradient; PME, particle mesh Ewald; GAFF, general Amber force field.

Chart 2. General Structure of the New Compounds

Scheme 1^{a,b}

^a Reagents and conditions: (a) β -alanine ethyl ester hydrochloride, WSC, HOBT, TEA, THF, room temp, 24 h, 96%; (b) MeI, CH₃CN, K₂CO₃, reflux, 30 h, 72%; (c) LiOH·H₂O, EtOH, room temp, 48 h, 89–94%; (d) PPA, 95 °C, 90 min to 6 h, 45–68%; (e) NaH, DMF, PMBCl, room temp, 4 h, 50%. (f) For **8b**: **7a**, MeI, NaH, DMF, room temp, 2 h, 40%. For **8c**: **7b**, PMBCl, NaH, DMF, room temp, overnight, 33%. (g) (CF₃SO₂)₂O, Na₂CO₃, CH₂Cl₂, room temp, 3–12 h, 26–75%; (h) *p*-HO-PhB(OH)₂, Pd(PPh₃)₄, toluene, NaHCO₃, EtOH, 60–90 min, 12–78%; (i) TFA, reflux, 5 h, 49%. ^b See Table 1.

binding site of some kinases (e.g., FGFR) in the *Z* configuration.²¹ The equilibrium favoring the *E* configuration could account for the low potency of RPI-1. In an attempt to improve the inhibitory properties of indolinone-related compounds, this study was undertaken to modify the indolinone scaffold maintaining the critical interactions within the RET kinase domain.

On these bases, we designed a series of 3,10-dihydro-2*H*-azepino[3,4-*b*]indol-1-ones (**1**) and of 4- (**2**) and 3-substituted β -carbolin-2-ones (**3**) that showed a satisfactory superimposition of the structural features deemed important for activity with those of both diastereoisomers of RPI-1, i.e., the 5,6-dimethoxy-

indole moiety and the carbonyl group. Furthermore, for the compounds of the **1** and **2** series there was also a good superimposition for the phenyl group. Some 3-aryl β -carbolin-1-ones derivatives have already been reported by Wang and co-workers as potent inhibitors of tumor cell proliferation, when substituted with electron-withdrawing substituents in the indole ring.²² The general structure of compounds in this series is reported in Chart 2, and the three-dimensional models of representative compounds appear in Figure 1. The new compounds were evaluated as RET inhibitors using cell-based and biochemical assays, and the docking mode of selected compounds was investigated by molecular modeling.

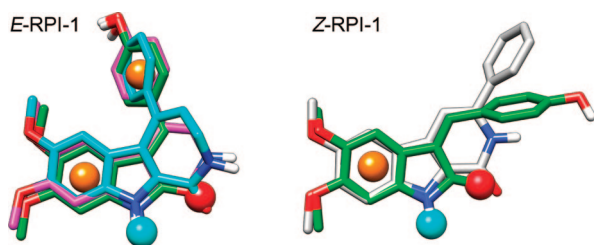
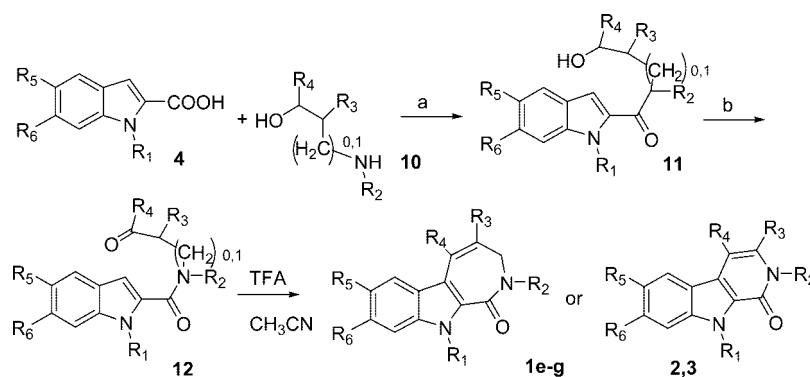


Figure 1. Superimposition between RPI-1 (colored green) and the new compounds (**1a**, **2a**, and **3a**, colored cyan, magenta, and gray, respectively). The most important pharmacophoric features are also reported (aromatic and hydrogen bond acceptor and donor features are reported as orange, red, and cyan spheres, respectively).

Chemistry

For the synthesis of the 3,10-dihydro-2*H*-azepino[3,4-*b*]indol-1-ones (**1**) we first followed a procedure described by Mérou²³ that was based on a palladium-mediated Suzuki reaction of an appropriate arylboronic acid with the enol triflate of an azepino[3,4-*b*]indole-1,5-dione (**9**) (Scheme 1). The latter was obtained by PPA cyclization of the acid **6**, in turn prepared by amidation of a substituted indole-2-carboxylic acid (**4**) with β -alanine ethyl ester hydrochloride, followed by hydrolysis with lithium hydroxide.

In our hands, triflation of the azepinedione **7a** gave a mixture of compounds triflated on the amide and indole NHs. Therefore compounds **1a–d** were only obtained by protecting the amide

Scheme 2^a

^a For R₁–R₆, see Table 1. Reagents and conditions: (a) WSC, HOBT, THF, room temp; (b) IBX, EtOAc, 80 °C or PCC, CH₂Cl₂, 40–50 °C; (c) TFA, CH₃CN, 80 °C.

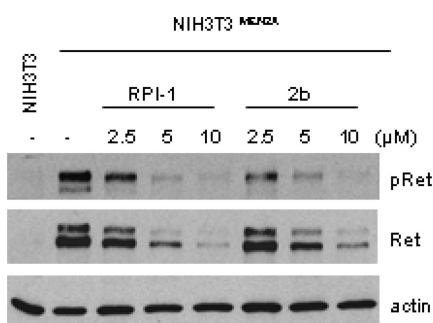


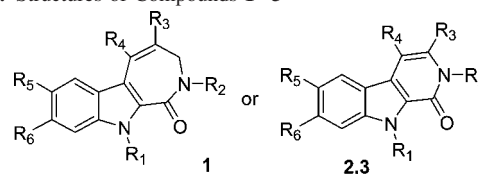
Figure 2. Inhibition of RET autophosphorylation and expression in NIH3T3^{MEN2A} cells treated with compound **2b** or RPI-1 as reference compound. Cells were exposed to vehicle (DMSO) or to the indicated concentrations of the compounds for 24 h. Whole cell lysates were analyzed by Western blotting with anti-p(Y1062)Ret and anti-Ret antibodies. A cell extract from untreated parental NIH3T3 cells was run in parallel. Anti-actin blot is shown as protein loading control.

or the indole NH with a methyl or a 4-methoxybenzyl group (**8b,c**). Because of these difficulties, we designed a more straightforward and general method that could be applied also to the synthesis of 5-alkyl substituted azepinoindol-1-ones and to the synthesis of compounds **2** and **3**. Appropriate indole-2-carboxylic acids were coupled with β - or γ -aminoalcohols to obtain, after IBX oxidation, β - or γ -oxoamides that were cyclized via an intramolecular Friedel–Crafts reaction to give directly the expected compounds **1–3** (Scheme 2). Alternatively, condensation with β - or γ -aminoketones gave directly the oxoamides ready for cyclization. This approach has been recently disclosed and used for the synthesis of compounds **2** and **3**.²⁴ The synthesis of N-unsubstituted derivatives required the use of an appropriate R₁ protecting group.

Results and Discussion

Cellular and Biochemical Studies. To assess the effect of the new compounds on RET-driven cellular transformation, we tested their ability to affect the proliferation and/or the transformed morphologic phenotype of NIH3T3 cells stably transfected with the C634R mutant of RET associated with the MEN2A syndrome (NIH3T3^{MEN2A}).^{2,3} Compounds that showed an antiproliferative activity comparable to that displayed by the reference molecule RPI-1 or showed an ability to revert the morphology of the transformed phenotype were further tested on NIH3T3 and NIH3T3 cells transformed with a non-tyrosine kinase oncogene (NIH3T3^{H-RAS}) to assess the drug selectivity against RET-oncogene-expressing cells. Compounds exhibiting these features belong to the series **2**. Compounds of the series

Table 1. Structures of Compounds **1–3**



compd	R ₁	R ₂	R ₃	R ₄	R ₅	R ₆
1a	H	H	H	4-OH-Ph	OCH ₃	OCH ₃
1b	CH ₃	H	H	4-OH-Ph	OCH ₃	OCH ₃
1c	CH ₃	CH ₃	H	4-OH-Ph	OCH ₃	OCH ₃
1d	CH ₃	PMB ^a	H	4-OH-Ph	OCH ₃	OCH ₃
1e	CH ₃	H	H	H	OCH ₃	OCH ₃
1f	CH ₃	H	H	CH ₃	OCH ₃	OCH ₃
1g	CH ₃	H	H	4-OCH ₃ -Ph	OCH ₃	OCH ₃
2a	H	H	H	4-OH-Ph	OCH ₃	OCH ₃
2b	CH ₃	H	H	4-OH-Ph	OCH ₃	OCH ₃
2c	CH ₃	H	H	4-OH-Ph	H	H
2d	CH ₃	H	H	4-OH-Ph	OCH ₃	H
2e	CH ₃	CH ₂ -Ph	H	H	OCH ₃	OCH ₃
2f	CH ₃	H	H	CH ₃	OCH ₃	OCH ₃
2g	CH ₃	H	H	Ph	OCH ₃	OCH ₃
2h	CH ₃	H	H	3-OH-Ph	OCH ₃	OCH ₃
2i	CH ₂ -Ph	H	H	4-OH-Ph	OCH ₃	OCH ₃
3a	H	H	Ph	H	OCH ₃	OCH ₃
3b	CH ₃	H	Ph	H	OCH ₃	OCH ₃
3c	Naf-2-CH ₂	H	Ph	H	H	H

^a PMB = 4-methoxybenzyl.

1 and **3** were characterized by a lower potency and by lack of revertant activity. Therefore, only compounds of the series **2** were further subjected to a RET kinase assay to assess direct enzyme inhibition. The inhibition of RET activation in treated NIH3T3^{MEN2A} cells was eventually examined by Western blotting.

The results of the cell-based screening with the new compounds are reported in Table 2, together with RET kinase inhibition data for selected molecules.

Compounds with structure **1**, characterized by a seven-membered azepinoindolone ring fused to an indole moiety, showed in general a lower antiproliferative activity than the reference compound against NIH3T3^{MEN2A} cells and no revertant capacity. In contrast, compounds with structure **2**, in particular **2a,b** and **2f–h**, appeared to be comparable to the reference compound RPI-1 as for the activity on NIH3T3^{MEN2A} cells. In addition, some of them (**2a** and **2b**) induced a partial or transient reversion of the transformed morphology of these cells. Similar to RPI-1, **2a** and **2b** showed a selective antiproliferative activity against NIH3T3 cells expressing the RET mutant. Moreover, the remarkable inhibitory activity in the RET kinase assay by both compounds suggested that the lack of *N*-methyl in the indole

Table 2. In Vitro Activity of Compounds 1–3

compd	antiproliferative activity (IC ₅₀ μM) ^a (72 h)			RET KA ^d (IC ₅₀ μM)
	NIH3T3 ^{MEN2A}	NIH3T3	NIH3T3 ^{H-RAS}	
RPI-1	3.6 ± 1.6 ^b	16.3 ± 3.7	19.7 ± 2	0.16 ± 0.05
1a	19.8 ± 7.1			
1b	14.4 ± 5.5			
1c	18.4 ± 3			
1d	6.8 ± 2.5			
1e	7.8 ± 2			>0.6
1f	16.7 ± 5.4			
1g	9.9 ± 1.2			
2a	4.7 ± 0.3 ^c	13.9 ± 2	13.5 ± 0.3	0.11 ± 0.04
2b	1.95 ± 0.2 ^c	7.2 ± 2.2	6.6 ± 2	0.06 ± 0.02
2c	17.3 ± 1.1	>30	>30	0.48 ± 0.12
2d	12.2 ± 1 ^c	25 ± 8	>30	0.60 ± 0.01
2e	15.9 ± 2.6			>0.6
2f	5.6 ± 0.04	10.6 ± 2.5		>0.6
2g	3.3 ± 0.6	17.8 ± 0.1	13.8 ± 2.8	0.25 ± 0.1
2h	3.2 ± 0.3 ^c	6.7 ± 0.1	6.1 ± 2	0.09 ± 0.01
2i	7.5 ± 1	17.7 ± 0.6		
3a	13.3 ± 1			
3b	34.4 ± 1.2			
3c	18.4 ± 0.8			

^a Mean values ± SD from at least two independent experiments performed in duplicate are reported. ^b Stable reversion of transformed morphology of NIH3T3^{MEN2A} cells exposed to 10 μM RPI-1. ^c Partial or transient reversion of transformed morphology of NIH3T3^{MEN2A} cells observed during drug treatment. ^d Kinase assay using recombinant RET active protein and MBP as a substrate.

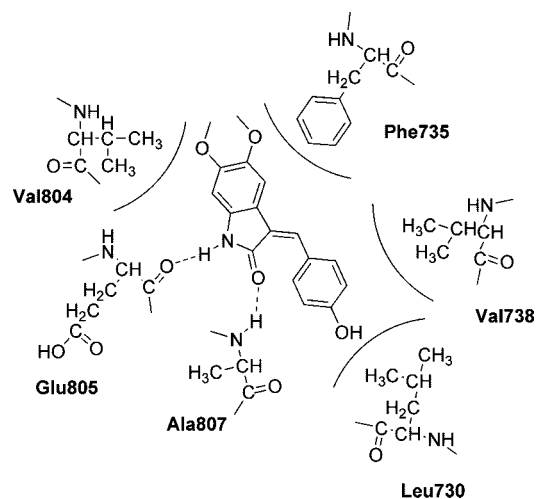
moiety did not abrogate the enzyme inhibitory activity. These findings were apparently (but see later) in contrast with the results previously obtained in a series of analogues of the indolin-2-one RPI-1²⁵ in which the presence of *N*-methyl in the indole moiety was found to abrogate the inhibitory activity.

The low antiproliferative activity of compounds **2c,d** could be explained by the lack of one or both the methoxy groups on the indole moiety, a detrimental effect already observed in the indolinone series.²⁵ Despite the deletion of the phenolic OH, compound **2g** maintained the antiproliferative effect with only a slight reduction of the inhibitory activity on recombinant enzyme. At variance, deletion of the whole phenolic ring (**2f**) heavily impaired the enzyme inhibitory activity. Finally, compounds of structure **3**, intended to mimic the *Z*-isomer of RPI-1, were much less active.

The RET inhibitory activity of compound **2b**, identified as the best inhibitor in these series, was further confirmed on NIH3T3^{MEN2A} intact cells. Accordingly to the relative activity in the Ret kinase assay, **2b** inhibited Ret tyrosine phosphorylation in a dose-dependent way showing a slightly higher potency, compared to RPI-1, upon 24 h of cell treatment. As previously reported for RPI-1,⁷ RET kinase inhibition in treated cells was associated with a reduction of Ret protein expression (Figure 2).

Molecular Modeling. Since the present results seemed in apparent contrast with previous studies, suggesting a preferential or exclusive role of the *Z* isomer of indolinone molecules for the tyrosine kinase inhibitory activity,^{19–21} we investigated the binding interactions between the new derivatives and the RET tyrosine kinase domain. An automated docking analysis of compounds reported in Table 1 was performed into the crystallographic structure of RET kinase (PDB code 2ivu²⁶) using GOLD 3.2 software.²⁷

The parameters chosen in GOLD (see Experimental Section) were tested for their ability to reproduce the crystallized binding geometry of the 4-anilinoquinazoline ZD6474. The docking software easily found the binding geometry corresponding to the crystallized complex among the solutions with the lowest

**Figure 3.** Schematic representation of the main interactions of *Z*-RPI-1 into the RET binding site.

energy, with a root-mean-square deviation (rmsd) between the docked and crystallized geometries in the limit of the crystallographic resolution (the rmsd was less than 1.4 Å, whereas the crystallographic resolution was greater than 2.5 Å).

We have already reported the docking of the reference compound RPI-1, and our previous studies suggested that the active diastereoisomer has the *Z* configuration.²⁰ Figure 3 shows a schematic representation of the main interactions of this ligand inside the RET ATP binding site, with the indolin-2-one central scaffold that formed two H-bonds with the backbone of Glu805 and Ala807, respectively. These two interactions were supported by the analysis of the X-ray complexes between different kinases and inhibitors interacting in the ATP binding site²⁸ and by pharmacophoric studies.²⁹ Such studies confirmed in fact that the backbone portion of these two residues play a role in inhibitor binding, as they make H-bonds with N-1 and N-6 of the ATP adenine, as well as with most kinase inhibitors. With regard to the lipophilic interactions, the indolin-2-one group mainly interacted with Phe735, Val738, and Val804 whereas the phenolic substituent interacted with Leu730.

Figure 4A shows the docking of compound **2a**. Its interactions were indeed completely different from those hypothesized in the design step; the nitrogen and the oxygen of the pyridone ring formed H-bonds with the backbone of key residues Glu805 and Ala807, respectively. The planar 2H-pyrido[3,4-*b*]indol-1(9*H*)-one central scaffold mainly interacted with Leu730, Val738, Ala756, and Leu881, while the nitrogen of the indole moiety seemed devoid of important interactions. As for the 4-(*p*-hydroxyphenyl) substituent, it was inserted into a pocket delimited by Leu779, Ile788, Val804, and Ser891 and the hydroxy group formed an H-bond with Asp892 that constitutes an H-bond network with Lys758 and Glu775.

The docking studies highlighted that the 3-substitution determined the weakening of the H-bond between the oxygen of the pyridone ring and Ala807 and the loss of the H-bond between the nitrogen of the pyridone ring and Glu805 (see docking of compound **3a** in Figure 4B). Finally the docking of compound **1a** (Figure 4C) revealed that the change of geometry due to the seven-membered structure of the azepine ring fused to the indole determined a completely different binding mode, with the formation of two H-bonds with D892 and the loss of the fundamental interactions with the key residues Glu805 and Ala807.

As shown in Figure 5A, the docking of compound **2b**, which differs from **2a** (Figure 4A) only for the methyl substitution on

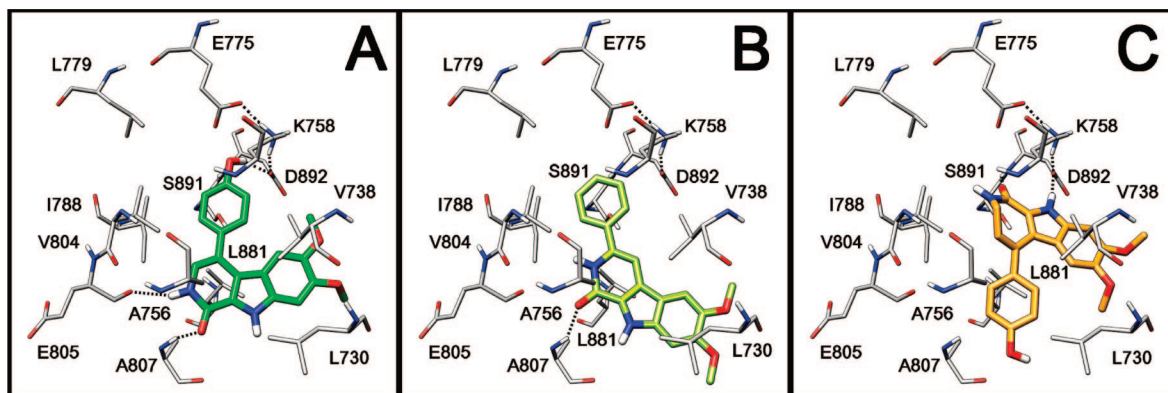


Figure 4. Docking of compounds **2a** (A), **3a** (B), and **1a** (C) into the RET binding site.

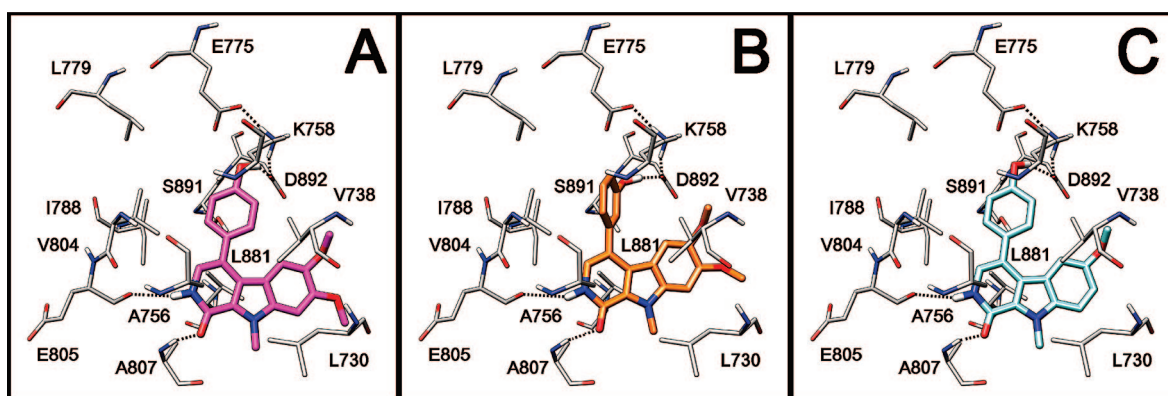


Figure 5. Docking of compounds **2b** (A), **2h** (B), and **2d** (C) into the RET binding site.

the indole nitrogen, highlighted the same binding disposition and the same interactions described above. Furthermore, the *N*-methyl substituent showed lipophilic interactions with Leu730.

Figure 5B shows the docking of compound **2h** which differs from compound **2b** (Figure 5A) for the 4-(*m*-hydroxyphenyl) substituent. In agreement with a profile of activity in the antiproliferative and biochemical tests very similar to that of **2b**, it showed all the main interactions of **2b**, in particular the H-bond between the phenolic OH group and Asp892.

Finally, compounds **2c** and **2d** are both characterized by the absence of the 7-methoxy substituent, and their low activity seemed to suggest a role for this group. However, in all the already mentioned compounds, this substituent did not show any important interaction with the enzyme and was exposed to the solvent. As shown in Figure 5C, compound **2d** showed the same interaction scheme; it possessed all the main interactions of the other compounds, and the 7-methoxy substituent was exposed to the solvent. Therefore, these data suggested that its lower affinity could be determined by different solvation effects.

In order to investigate this hypothesis, compounds **2b** and **2d** were subjected to 1 ns of molecular dynamics (MD) simulation with explicit water, followed by a molecular mechanics generalized Born surface area (MM-GBSA) analysis.³⁰ This approach has been shown to be able to estimate the ligand–receptor energy interaction.^{31–35} It averages contributions of gas-phase energies and solvation free energies calculated for snapshots of the complex molecule as well as the unbound components, extracted from MD trajectories according to the procedure fully described in the Experimental Section.

As shown in Figure 6A, after 200 ps of MD, both complex systems reached equilibrium, since the total energy for the

remaining simulation time was constant. Analyzing the rmsd from the X-ray structure of all the heavy atoms of the complexes, we observed that, after an initial increase, the rmsd did not exceed the value of 1.4 Å (see Figure 6B), suggesting that our MD procedure was correct.

As regard the two ligands, during the whole MD simulation their relative position appeared to change only slightly, since the rmsd of the heavy atoms of the ligands between the starting and the final structures of the MD simulation was 1.2 Å for **2b** and 1.1 Å for **2d**.

As shown in Table 3, the two ligands possessed a very similar binding interaction scheme: the nitrogen and the oxygen of the pyridone ring of both ligands maintained the H-bond with the backbone of Glu805 and Ala807, respectively, the 4-(*p*-hydroxyphenyl) substituent maintained an H-bond with the network constituted by Lys758 and Glu775 and Asp892, but instead of interacting with the carboxylic group of Asp892, it formed an H-bond with Glu775 and occasionally interacted with the backbone of Asp892.

The two MD trajectories were then analyzed through the MM-GBSA method. As shown in Table 4, the molecular mechanical energy (ΔE_{MM}) of the interaction of the ligands with RET (i.e., the sum of the electrostatic and van der Waals energies) was very similar for both compounds. However, the solvation free energy (ΔG_{Sol}), which includes the polar solvation free energy calculated with the generalized Born (GB) approximation model and the nonpolar part obtained by fitting solvent accessible surface area (SASA), was more favorable for compound **2b**. Therefore, even if the energy difference between the interaction of the two compounds was in the same order of magnitude of the standard deviation of error (see Table 4), the effect of the

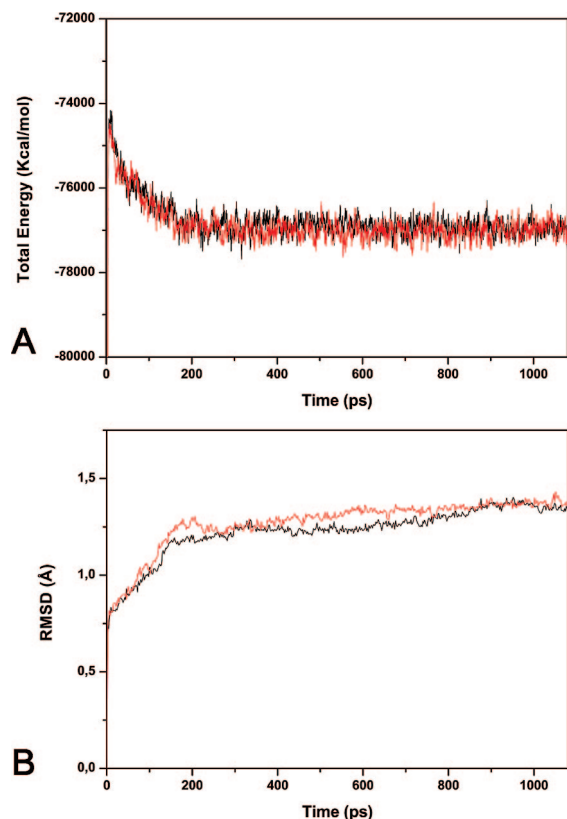


Figure 6. Results of the MD simulation of compounds **2b** (black) and **2d** (red) complexed with RET: (A) total energy (kcal/mol) of the system plotted versus time (ps); (B) rmsd in angstroms (Å), between the protein and the starting X-ray structure for all the heavy atoms, versus time (ps).

Table 3. Hydrogen Bonds Analysis of **2b** and **2d** with RET during the Simulation of Both Complexes

donor	acceptor H	acceptor	distance (Å)	% occupied
2b (R = OCH ₃)				
E775@OE2	LIG@H1	LIG@O1	2.63 (0.11)	97.0
E805@O	LIG@N2	LIG@H2	2.70 (0.19)	94.6
LIG@O3	A807@H	A807@N	2.83 (0.22)	94.1
LIG@O1	D892@H	D892@N	3.10 (0.16)	54.4
2d (R = H)				
LIG@O3	A807@H	A807@N	2.79 (0.09)	100
E805@O	LIG@N2	LIG@H2	2.92 (0.12)	99.8
E775@OE2	LIG@H1	LIG@O1	2.58 (0.10)	98.0
LIG@O1	D892@H	D892@N	3.11 (0.16)	54.1

7-methoxy substituent on the activity could be explained in terms of solvation free energy, in agreement with our hypothesis.

Conclusions

The results reported above indicate that compounds with structure **2** (e.g, **2a**, **2b**, and **2h**) exhibit a remarkable inhibitory

Table 4. MM-GBSA Results for Compounds **2b** and **2d**^a

	2b (STD)	2d (STD)
Ele	-41.9 (4.1)	-42.9 (3.8)
VdW	-38.0 (3.4)	-36.5 (3.6)
E_{int}	0.0 (0.0)	0.0 (0.0)
ΔE_{MM}	-79.9 (3.9)	-79.4 (4.3)
GB _{Sur}	-5.8 (0.1)	-5.3 (0.1)
GB	41.1 (1.9)	42.7 (2.3)
ΔGB_{Solv}	35.3 (1.9)	37.4 (2.3)
ΔG_{GBSA}	-44.6 (3.1)	-42.0 (3.5)

^a ΔE_{MM} is the sum of the electrostatic (Ele), van der Waals (VdW), and internal (E_{int}) energies. ΔGB_{Solv} is the sum of the polar (GB) and nonpolar (GB_{Sur}) solvation free energy. Finally ΔG_{GBSA} is the sum of the molecular mechanical and solvation free energy. STD means the standard deviation. Data are expressed as kcal/mol.

activity against the RET protein kinase, which is correlated with an antiproliferative activity on NIH3T3^{MEN2A} cells comparable to that of the reference compound RPI-1 which is correlated with a revertant activity on NIH3T3^{MEN2A} cells. No precise correlations between inhibitory activity against RET kinase and antiproliferative activity could be detected for compounds of this series because it is likely that the cell growth inhibition reflects inhibitory effects on multiple targets. Nonetheless, compounds of series **2** showed a preferential antiproliferative activity on RET mutant-expressing cells. As for SAR, it appears that methylation of the indole nitrogen is not detrimental but seems to increase the activity (**2b** vs **2a**). The presence of the two methoxy groups in positions 6 and 7 of the indole moiety is important in maintaining the activity, and the presence of a 3- or 4-OH substituted phenyl ring in position 4 is also beneficial, compound **2b** being the most active, on both the enzyme and cells. All these results are well explained by the analysis of the docking of the compounds in the crystallographic model of the enzyme. The same analysis also explains the lack of activity of compounds with structure **3**, where the ring attached to position 3 seems devoid of favorable interactions. For these reasons, this latter group of compounds was not investigated further. The same could be possible for compounds of structure **1**, where most probably the change of geometry due to the seven-membered structure of the azepine ring fused to the indole moves the substituent in position 5 to another zone of unfavorable interactions.

The compounds structurally most similar to the isomer *E* of RPI-1, i.e., **2a** and **2b**, are the most active of the series. At first glance, this finding could have appeared surprising, since on the basis of previous studies, the isomer *Z* is likely responsible of the inhibitory effects.²¹ However, considering the results of the present docking analysis, the strong H-bond interactions with Glu805 and Ala807 of the enzyme ATP binding site do not occur with the indole NH and the CO amide groups of **2**, as we hypothesized, but with the amide NH and CO groups of the pyridone ring. The consequence is that the compounds dock themselves in the binding site in a position flipped of roughly 180° with respect to RPI-1, and the phenolic OH in position 4 of **2a** and **2b** interacts with amino acids different from those interacting with RPI-1. The docking analysis also explains the slightly better inhibitory activity of **2b** vs **2a** in the kinase assay, on the basis of the absence of H-bond interactions with the indole NH and of the existence of lipophilic interactions with Leu730. Notably, in spite of the different binding mode to the RET kinase, compound **2b** maintained the ability to inhibit RET protein expression, in addition to tyrosine phosphorylation, as previously described for RPI-1.⁷

In conclusion, we have found a new series of inhibitors of RET protein kinase with an inhibitory and antiproliferative

activity comparable to that of RPI-1, which may provide a new lead candidate. Since this series is characterized by lack of changes of configuration, the rigid structure could provide biochemical and pharmacological advantages over conventional indolinones.

Experimental Section

General Chemical Methods. All reagents and solvents were reagent grade or were purified by standard methods before use. Melting points were determined in open capillaries on a Büchi melting point apparatus and are uncorrected. Column chromatography was carried out on flash silica gel (Merck 230–400 mesh). TLC analysis was conducted on silica gel plates (Merck 60F₂₅₄). NMR spectra were recorded at 300 MHz with a Bruker instrument. Chemical shifts (δ values) and coupling constants (J values) are given in ppm and Hz, respectively. Compounds **2** and **3** were prepared as already described.²⁴

3-[(5,6-Dimethoxy-1H-indole-2-carbonyl)amino]propionic Acid Ethyl Ester (5a). A solution of 5,6-dimethoxy-1H-indole-2-carboxylic acid (1.46 g, 6.6 mmol), EDC (1.52 g, 7.9 mmol), and HOBT (1.07 g, 7.9 mmol) in 36 mL of THF was stirred 8 h at room temperature. Then β -alanine ethyl ester hydrochloride (3.04 g, 19.8 mmol) and TEA (2.74 mL, 19.8 mmol) were added. The mixture was stirred overnight at room temperature. After partial evaporation of the solvent, water and HCl 10% (12 mL) were added. The precipitate was filtered to give 2.02 g of the title compound. Yield 96%. ¹H NMR (300 MHz, CDCl₃) δ : 9.15 (1H, NH), 7.00 (s, 1H, 1 Ar), 6.82 (s, 1H, 1 Ar), 6.65–6.75 (m, 2H, CH= + NHCO), 4.20 (q, 2H, OCH₂, J = 7.1 Hz), 3.98 (s, 3H, OMe), 3.95 (s, 3H, OMe), 3.65–3.75 (m, 2H, CH₂N), 2.65 (t, 2H, CH₂, J = 6.9 Hz), 1.25 (t, 3H, CH₃, J = 7.1 Hz). Anal. (C₁₆H₂₀N₂O₅) C, H, N.

3-[(5,6-Dimethoxy-1-methyl-1H-indole-2-carbonyl)amino]propionic Acid Ethyl Ester (5b). To a solution of **5a** (500 mg, 1.56 mmol) in 25 mL of acetonitrile, K₂CO₃ (970 mg, 7.02 mmol) and MeI (554 mg, 3.9 mmol) were added. The solution was refluxed for 30 h. Then the precipitate was filtered and the solvent evaporated. The residue was dissolved in CH₂Cl₂ and washed with 40 mL of 1 N HCl. The organic layer was dried over Na₂SO₄ and evaporated in vacuo. The crude residue was purified by column chromatography (eluent, hexane/ethyl acetate 35:65) to afford **5b**. Yield 72%, mp 135 °C. ¹H NMR (CDCl₃) δ : 7.00 (s, 1H, 1 Ar), 6.76 (s, 1H, 1 Ar), 6.73 (s, 1H, 1 Ar), 4.17 (q, 2H, OCH₂, J = 7.1 Hz), 4.01 (s, 3H, OMe), 3.96 (s, 3H, OMe), 3.90 (s, 3H, NMe), 3.64–3.70 (m, 2H, CH₂), 2.60–2.68 (m, 2H, CH₂), 1.27 (t, 3H, CH₃, J = 7.1 Hz). Anal. (C₁₇H₂₂N₂O₅) C, H, N.

3-[(5,6-Dimethoxy-1H-indole-2-carbonyl)amino]propionic Acid (6a). To a suspension of **5a** (1 g, 3.12 mmol) in 55 mL of EtOH was added LiOH·H₂O (0.262 g, 6.24 mmol), and the mixture was stirred for 48 h at room temperature. After evaporation of the solvent, the residue was dissolved in water and cold concentrated HCl was dropped during 15 min under stirring. The precipitate was filtered to obtain 810 mg of the title compound. Yield 89%, mp 245 °C. ¹H NMR (DMSO-*d*₆) δ : 12.25 (br s, 1H, COOH), 11.26 (s, 1H, NH), 8.26 (t, 1H, NH, J = 5.2 Hz), 7.05 (s, 1H, 1Ar), 6.96 (s, 1H, 1 Ar), 6.87 (s, 1H, 1Ar), 3.76 (s, 3H, OMe), 3.75 (s, 3H, OMe), 3.4–3.5 (m, 2H, CH₂), 2.45–2.55 (m, 2H, CH₂). Anal. (C₁₄H₁₆N₂O₅) C, H, N.

3-[(5,6-Dimethoxy-1-methyl-1H-indole-2-carbonyl)amino]propionic Acid (6b). To a suspension of **5b** (378 mg, 1.13 mmol) in 20 mL of EtOH was added LiOH·H₂O (96 mg, 2.26 mmol), and the mixture was stirred for 48 h at room temperature. After evaporation of the solvent, the residue was dissolved in water and cold 6 N HCl was dropped during 15 min under stirring. The white precipitate was filtered to obtain 324 mg of the title compound. Yield 94%, mp 200 °C. ¹H NMR (DMSO-*d*₆) δ : 12.23 (s, 1H, COOH), 8.34 (t, 1H, NH, J = 5.9 Hz), 7.07 (s, 1H, 1 Ar), 7.03 (s, 1H, 1Ar), 6.94 (s, 1H, 1Ar), 3.94 (s, 3H, OMe), 3.83 (s, 3H, OMe), 3.76 (s, 3H, NMe), 3.3–3.5 (m, 2H, CH₂), 2.45–2.55 (m, 2H, CH₂). Anal. (C₁₅H₁₈N₂O₅) C, H, N.

7,8-Dimethoxy-3,4-dihydro-2H,10H-azepino[3,4-*b*]indole-1,5-dione (7a). A mixture of **6a** (0.76 g, 2.6 mmol) and PPA (58 g) was stirred at 95 °C for 6 h. After the mixture was cooled, iced water was added and the aqueous phase was continuously extracted with a solution CH₂Cl₂/MeOH 95:5. Purification by flash chromatography (eluent, CH₂Cl₂/MeOH 95:5) afforded the title compound in a 45% yield. ¹H NMR (DMSO-*d*₆) δ : 12.20 (s, 1H, NH), 8.68 (t, 1H, CONH, J = 5.9 Hz), 7.75 (s, 1H, 1 Ar), 6.99 (s, 1H, 1Ar), 3.78 (s, 6H, 2OMe), 3.3–3.5 (m, 2H, CH₂), 2.75–2.85 (m, 2H, CH₂). Anal. (C₁₄H₁₄N₂O₄) C, H, N.

7,8-Dimethoxy-10-methyl-3,4-dihydro-2H,10H-azepino[3,4-*b*]indole-1,5-dione (7b). A mixture of **6b** (324 mg, 1.06 mmol) and PPA (13 g) was stirred at 90 °C for 90 min. After the mixture was cooled, an amount of 50 mL of iced water was added and the aqueous phase was extracted with CH₂Cl₂. The organic layer was dried over Na₂SO₄ and evaporated in vacuo to afford 208 mg of the title compound. Yield 68%. ¹H NMR (DMSO-*d*₆) δ : 8.65 (t, 1H, CONH, J = 5.9 Hz), 7.74 (s, 1H, 1Ar), 7.19 (s, 1H, 1Ar), 3.99 (s, 3H, 2OMe), 3.87 (s, 3H, OMe), 3.80 (s, 3H, NMe), 3.45–3.50 (m, 2H, CH₂), 2.72–2.78 (m, 2H, CH₂). Anal. (C₁₅H₁₆N₂O₄) C, H, N.

7,8-Dimethoxy-10-(4-methoxybenzyl)-3,4-dihydro-2H,10H-azepino[3,4-*b*]indole-1,5-dione (7c). A suspension of **7a** (0.843 g, 3.07 mmol) in DMF (15.2 mL) was cooled to 0 °C. Then NaH (60% in mineral oil, 0.843 g, 7.37 mmol) was added. The solution was stirred for 1 h at room temperature. Then PMBCl (1.19 g, 7.37 mmol) was dropped and stirring was continued for further 3 h. The mixture was added to water and extracted twice with dichloromethane. The organic layer was dried over Na₂SO₄ and evaporated in vacuo. Flash chromatography (eluent from ethyl acetate/hexane 85:15 to ethyl acetate) afforded **7c**. Yield 50%, mp 260 °C. ¹H NMR (DMSO-*d*₆) δ : 8.69 (t, 1H, CONH, J = 5.9 Hz), 7.73 (s, 1H, 1 Ar), 7.18 (s, 1H, 1 Ar), 7.11 (d, 2H, 2Ar, J = 8.6 Hz), 6.84 (d, 2H, 2Ar, J = 8.6 Hz), 5.82 (s, 2H, CH₂Ph), 3.79 (s, 6H, 2OMe), 3.69 (s, 3H, OMe), 3.3–3.4 (m, 2H, CH₂), 2.74–2.82 (m, 2H, CH₂). Anal. (C₂₂H₂₂N₂O₅) C, H, N.

7,8-Dimethoxy-2,10-dimethyl-3,4-dihydro-2H,10H-azepino[3,4-*b*]indole-1,5-dione (8b). To a suspension of **7a** (314 mg, 1.14 mmol) in DMF (4.35 mL), NaH (60% in mineral oil, 65 mg, 2.69 mmol) was added. The solution was stirred for 1 h at room temperature, and then MeI (389 mg, 2.74 mmol) was dropped and stirring was continued for 1 h. The mixture was added to water and extracted twice with dichloromethane. The organic layer was dried over Na₂SO₄ and evaporated in vacuo. Flash chromatography (eluent, CH₂Cl₂/MeOH 98:2) afforded **8b**. Yield 40%, mp 182 °C. ¹H NMR (CDCl₃) δ : 7.82 (s, 1H, 1Ar), 6.82 (s, 1H, 1Ar), 4.02, 3.95, 3.95, (2s, 9H, 2OMe and NMe), 3.7–3.8 (m, 2H, CH₂), 3.25 (s, 3H, NMe), 2.8–2.9 (m, 2H, CH₂). Anal. (C₁₆H₁₈N₂O₄) C, H, N.

7,8-Dimethoxy-2-(4-methoxybenzyl)-10-methyl-3,4-dihydro-2H,10H-azepino[3,4-*b*]indole-1,5-dione (8c). A suspension of **7b** (205 mg, 0.71 mmol) in DMF (3.7 mL) was cooled to 0 °C, and then NaH (60% in mineral oil, 20.5 mg, 0.85 mmol) was added. The solution was stirred for 1 h at room temperature, and then PMBCl (138 mg, 0.85 mmol) was dropped and stirring was continued overnight. The mixture was added to water (6 mL) and extracted twice with ethyl acetate. The organic layer was dried over Na₂SO₄ and evaporated in vacuo. Flash chromatography (eluent, hexane/ethyl acetate 45:55) afforded the title compound as a white solid. Yield 33%. ¹H NMR (CDCl₃) δ : 7.80 (s, 1H, 1Ar), 7.30 (d, 2H, 2Ar, J = 8.5 Hz), 6.88 (d, 2H, 2Ar, J = 8.5 Hz), 6.79 (s, 1H, 1Ar), 4.77 (s, 2H, CH₂Ph), 4.09 (s, 3H, OMe), 3.99 (s, 3H, OMe), 3.95 (s, 3H, OMe), 3.76 (s, 3H, NMe), 3.65–3.75 (m, 2H, CH₂), 2.65–2.75 (m, 2H, CH₂). Anal. (C₂₃H₂₄N₂O₅) C, H, N.

Trifluoromethanesulfonic Acid 7,8-Dimethoxy-1-oxo-1,2,3,10-tetrahydroazepino[3,4-*b*]indol-5-yl Ester (9a). To a suspension of compound **7c** (290 mg, 0.735 mmol) and Na₂CO₃ (109 mg, 1.03 mmol) in dry CH₂Cl₂ (7.5 mL) was added trifluoromethanesulfonic anhydride (317 mg, 1.10 mmol). The mixture was stirred for 3 h at room temperature. Then water was added and the aqueous phase was extracted with CH₂Cl₂. The organic layer was dried over

Na₂SO₄ and evaporated in vacuo. Flash chromatography (eluent CH₂Cl₂/MeOH 99.5:0.5) afforded **9a** (26%), mp >250 °C (dec). ¹H NMR (DMSO-*d*₆) δ: 12.87 (s, 1H, NH), 7.21 (s, 1H, 1Ar), 6.98 (s, 1H, 1Ar), 6.56 (t, 1H, CH=, *J* = 7.1 Hz), 4.5–4.6 (m, 2H, CH₂), 3.82 (s, 3H, OMe), 3.78 (s, 3H, OMe). Anal. (C₁₅H₁₃-F₃N₂O₆S) C, H, N.

Trifluoromethanesulfonic Acid 7,8-Dimethoxy-2,10-dimethyl-1-oxo-1,2,3,10-tetrahydroazepino[3,4-*b*]indol-5-yl Ester (9b). To a suspension of compound **8b** (127 mg, 0.42 mmol) and Na₂CO₃ (63.7 mg, 0.60 mmol) in dry CH₂Cl₂ (1.6 mL) was dropped a solution of trifluoromethanesulfonic anhydride (176 mg, 0.613 mmol) in CH₂Cl₂ (2.6 mL). The mixture was stirred at room temperature overnight. Then water was added and the aqueous phase was extracted with CH₂Cl₂. The organic layer was dried over Na₂SO₄ and evaporated in vacuo. Flash chromatography (eluent CH₂Cl₂/MeOH 99:1) afforded **9b** (75%), mp 96 °C. ¹H NMR (CDCl₃) δ: 7.31 (s, 1H, 1Ar), 6.80 (s, 1H, 1Ar), 6.09 (t, 1H, CH=, *J* = 7.1 Hz), 4.04 (s, 3H, OMe), 3.99 (s, 3H, OMe), 3.93 (s, 3H, NMe), 3.83 (d, 2H, CH₂N, *J* = 7.1 Hz), 3.28 (s, 3H, NMe). Anal. (C₁₇H₁₇F₃N₂O₆S) C, H, N.

Trifluoromethanesulfonic Acid 7,8-Dimethoxy-2-(4-methoxybenzyl)-10-methyl-1-oxo-1,2,3,10-tetrahydroazepino[3,4-*b*]indol-5-yl Ester (9c). To a suspension of compound **8c** (80 mg, 0.136 mmol) and Na₂CO₃ (29.1 mg, 0.274 mmol) in dry CH₂Cl₂ (1 mL) was dropped trifluoromethanesulfonic anhydride (84.6 mg, 0.294 mmol). The mixture was stirred at room temperature overnight, and then water was added and the aqueous phase was extracted with CH₂Cl₂. The organic layer was dried over Na₂SO₄ and evaporated in vacuo. Flash chromatography (eluent, hexane/ethyl acetate 55:45) afforded **9c** (28%), mp 190 °C. ¹H NMR (acetone-*d*₆) δ: 7.32 (d, 2H, 2Ar, *J* = 8.6 Hz), 7.29 (s, 1H, 1Ar), 7.18 (s, 1H, 1Ar), 6.89 (d, 2H, 2Ar, *J* = 8.6 Hz), 5.99 (t, 1H, CH=, *J* = 7.5 Hz), 4.76 (s, 2H, CH₂Ph), 4.06 (s, 3H, OMe), 3.94 (s, 3H, OMe), 3.89 (d, 2H, CH₂N, *J* = 7.5 Hz), 3.84 (s, 3H, NMe), 3.78 (s, 3H, NMe). Anal. (C₂₄H₂₃F₃N₂O₇S) C, H, N.

5-(4-Hydroxyphenyl)-7,8-dimethoxy-3,10-dihydro-2H-azepino[3,4-*b*]indol-1-one (1a). A solution of **9a** (375 mg, 0.222 mmol) and palladium tetrakis (15 mg) in 5 mL of toluene was stirred at room temperature for 3 h. Then a solution of 4-hydroxybenzeneboronic acid (46 mg, 0.33 mmol) in EtOH (2 mL) and a saturated solution of Na₂CO₃ (2 mL) were added. After the mixture was stirred for 90 min at 80 °C, brine was added and the mixture was extracted with ethyl acetate. The organic layer was dried over Na₂SO₄ and evaporated in vacuo. Flash chromatography (eluent, hexane/ethyl acetate 60:40) afforded **1a** (12%), mp 159 °C. ¹H NMR (acetone-*d*₆) δ: 11.25 (s, 1H, NH), 8.65 (s, 1H, CONH), 7.25 (d, 2H, 2Ar, *J* = 8.4 Hz), 7.08 (s, 1H, 1Ar), 6.91 (d, 2H, 2Ar, *J* = 8.4 Hz), 6.30 (t, 1H, CH=, *J* = 6.9 Hz), 6.01 (s, 1H, 1Ar), 4.45–4.55 (m, 2H, CH₂), 3.89 (s, 3H, OMe), 3.42 (s, 3H, OMe). Anal. (C₂₀H₁₈N₂O₄) C, H, N.

5-(4-Hydroxyphenyl)-7,8-dimethoxy-10-methyl-3,10-dihydro-2H-azepino[3,4-*b*]indol-1-one (1b). A solution of **1d** (130 mg, 0.27 mmol) in 10 mL of TFA was refluxed for 5 h. After evaporation of the solvent, a saturated solution of NaHCO₃ was added. The precipitate was filtered to obtain a crude that was purified by flash chromatography (eluent, CH₂Cl₂/MeOH 96:4). Yield 49%, mp >270 °C. ¹H NMR (DMSO-*d*₆) δ: 9.50 (s, 1H, OH), 8.18 (t, 1H, NHCO, *J* = 5.9 Hz), 7.10 (d, 2H, 2Ar, *J* = 8.4 Hz), 7.09 (s, 1H, 1Ar), 6.75 (d, 2H, 2Ar, *J* = 8.4 Hz), 6.01 (t, 1H, CH=, *J* = 6.9 Hz), 5.95 (s, 1H, 1Ar), 3.99 (s, 3H, OMe), 3.81 (s, 3H, OMe), 3.45 (m, 2H, CH₂), 3.30 (s, 3H, NMe). Anal. (C₂₁H₂₀N₂O₄) C, H, N.

5-(4-Hydroxyphenyl)-7,8-dimethoxy-2,10-dimethyl-3,10-dihydro-2H-azepino[3,4-*b*]indol-1-one (1c). A solution of **9b** (133 mg, 0.31 mmol) and palladium tetrakis (21 mg) in 7 mL of toluene was stirred at room temperature for 30 min. Then a solution of 4-hydroxybenzeneboronic acid (63 mg, 0.46 mmol) in EtOH (2.8 mL) and a saturated solution of Na₂CO₃ (2.8 mL) were added. After the mixture was stirred for 60 min at 80 °C, brine was added and the mixture was extracted with CH₂Cl₂. The organic layer was dried over Na₂SO₄ and evaporated in vacuo. Flash chromatography (eluent, hexane/ethyl acetate 35:65) afforded **1c** (49%), mp 228

°C. ¹H NMR (acetone-*d*₆) δ: 7.20 (d, 2H, 2Ar, *J* = 8.4 Hz), 7.08 (s, 1H, 1Ar), 7.85 (d, 2H, 2Ar, *J* = 8.4 Hz), 6.17 (t, 1H, CH=, *J* = 6.7 Hz), 6.11 (s, 1H, 1Ar), 4.01 (s, 3H, OMe), 3.89 (s, 3H, OMe), 3.84 (d, 2H, CH₂N, *J* = 6.7 Hz), 3.40 (s, 3H, NMe), 3.15 (s, 3H, NMe). Anal. (C₂₂H₂₂N₂O₄) C, H, N.

5-(4-Hydroxyphenyl)-7,8-dimethoxy-2-(4-methoxybenzyl)-10-methyl-3,10-dihydro-2H-azepino[3,4-*b*]indol-1-one (1d). A solution of **9c** (30 mg, 0.055 mmol) and palladium tetrakis (5 mg) in 1.26 mL of toluene was stirred at room temperature for 30 min. Then a solution of 4-hydroxybenzeneboronic acid (11.5 mg, 0.083 mmol) in EtOH (0.5 mL) and a saturated solution of Na₂CO₃ (0.5 mL) were added sequentially. After the mixture was stirred for 60 min at 80 °C, brine was added and the mixture was extracted with CH₂Cl₂. The organic layer was dried over Na₂SO₄ and evaporated in vacuo. Flash chromatography (eluent, hexane/ethyl acetate 50:50) afforded **1d** (78%), mp 193 °C. ¹H NMR (acetone-*d*₆) δ: 7.39 (d, 2H, 2Ar, *J* = 8.4 Hz), 7.18 (d, 2H, 2Ar, *J* = 8.4 Hz), 7.08 (s, 1H, 1Ar), 6.80–6.90 (m, 4H, 4Ar), 6.09 (s, 1H, 1Ar), 5.95 (t, 1H, CH=, *J* = 6.9 Hz), 4.71 (s, 2H, CH₂Ph), 4.06 (s, 3H, OMe), 3.90 (s, 3H, OMe), 3.75 (s, 6H, NMe and OMe), 3.38 (s, 3H, NMe). Anal. (C₂₉H₂₈N₂O₅) C, H, N.

5,6-Dimethoxy-1-methyl-1H-indole-2-carboxylic Acid (4b). To a solution of 5,6-dimethoxy-1H-indole-2-carboxylic acid ethyl ester (500 mg, 2 mmol) in CH₃CN (32 mL) were added K₂CO₃ (1.24 g, 9 mmol) and iodomethane (0.31 mL, 5 mmol), and the mixture was stirred at reflux for 13 h. The mixture was cooled to room temperature and filtered and the filtrate evaporated in vacuo. The solid was then washed with 1 N HCl and extracted with CH₂Cl₂, and the combined organic layers were dried over Na₂SO₄ and evaporated to give 480 mg (93%) of 5,6-dimethoxy-1-methyl-1H-indole-2-carboxylic acid ethyl ester, mp 148 °C. ¹H NMR (CDCl₃) δ: 7.17 (s, 1H), 7.00 (s, 1H), 6.75 (s, 1H), 4.53 (q, *J* = 7.5 Hz, 2H), 4.04 (s, 3H), 3.97 (s, 3H), 3.90 (s, 3H), 1.20 (q, *J* = 7.5 Hz, 3H). ¹³C NMR (75 MHz, CDCl₃) δ: 162.1, 149.8, 146.0, 134.9, 126.3, 118.6, 109.9, 102.4, 92.1, 60.2, 56.1, 56.0, 31.8, 14.4.

The above ester (0.48 mg, 1.8 mmol) was added to a solution of NaOH (2.90 g, 72.4 mmol) in ethanol (31.8 mL), and the mixture was refluxed for 2 h. Ethanol was evaporated to dryness in vacuo, the residue was dissolved in water, and the solution was acidified to pH 3 with 12 N HCl to form a yellow solid. The mixture was allowed to stand at 0 °C for 15 min, and the product was isolated by filtration (330 mg, 85%), mp 221 °C. ¹H NMR (DMSO-*d*₆) δ: 12.6 (br s, 1H), 7.10 (s, 1H), 7.08 (s, 1H), 7.05 (s, 1H), 4.00 (s, 3H), 3.87 (s, 3H), 3.78 (s, 3H). ¹³C NMR (75 MHz, DMSO-*d*₆) δ: 163.2, 149.9, 146.1, 135.1, 126.8, 118.4, 110.0, 103.0, 93.7, 56.1 (2C), 32.1. Anal. (C₁₂H₁₃NO₄) C, H, N.

5,6-Dimethoxy-1-methyl-1H-indole-2-carboxylic Acid (3-Hydroxypropyl)amide (11e). 3-Amino-1-propanol (121 μL, 1.59 mmol) was dissolved in dry THF (5.8 mL), and then EDC (311 mg, 1.59 mmol), HOBt (220 mg, 1.59 mmol), and **4b** (250 mg, 1.06 mmol) were added sequentially at room temperature. After the resulting mixture was stirred overnight, the solvent was removed and the crude product was poured into saturated aqueous NaHCO₃ and extracted with ethyl acetate. The combined organic layers were washed with 1 N HCl, saturated aqueous NaHCO₃, brine, dried over Na₂SO₄, and concentrated to give 210 mg (64%) of **11a**, mp 154 °C. ¹H NMR (DMSO-*d*₆) δ: 8.28 (t, *J* = 5.58 Hz, 1H), 7.07 (s, 1H), 7.03 (s, 1H), 6.92 (s, 1H), 4.57–4.45 (m, 1H), 3.95 (s, 3H), 3.84 (s, 3H), 3.76 (s, 3H), 3.55–3.44 (m, 2H), 3.29 (q, *J* = 6.70 Hz, 2H), 1.78 (q, *J* = 6.70 Hz, 2H). ¹³C NMR (75 MHz, DMSO-*d*₆) δ: 162.4, 148.8, 145.8, 133.9, 130.8, 118.5, 104.5, 103.0, 93.8, 59.1, 56.2, 56.1, 36.5, 32.9, 32.0. Anal. (C₁₅H₂₀N₂O₄) C, H, N.

5,6-Dimethoxy-1-methyl-1H-indole-2-carboxylic Acid (3-Hydroxybutyl)amide (11f). 4-Amino-2-butanol (206 μL, 2.12 mmol) was dissolved in dry THF (5.77 mL), and then EDC (415 mg, 2.12 mmol), HOBt (365 mg, 2.12 mmol), and **4b** (250 mg, 1.06 mmol) were added sequentially at room temperature. After the resulting mixture was stirred for 3 h under nitrogen, the solvent was removed and the crude product was poured into saturated aqueous NaHCO₃ and extracted with ethyl acetate. The combined organic layers were washed with 1 N HCl, saturated NaHCO₃, brine, dried over Na₂SO₄,

and concentrated to give 321 mg (99%) of **11b**, mp 162 °C. ^1H NMR (DMSO- d_6) δ : 8.26 (t, 5.95 Hz, 1H), 7.07 (s, 1H), 7.03 (s, 1H), 6.92 (s, 1H), 4.54 (d, J = 4.8 Hz, 1H), 3.94 (s, 1H), 3.83 (s, 1H), 3.76 (s, 1H), 3.74–3–62 (m, 1H), 3.30 (q, J = 5.9 Hz, 2H), 1.66–1.50 (m, 2H), 1.09 (d, J = 6.3 Hz, 3H). ^{13}C NMR (75 MHz, DMSO- d_6) δ : 162.3, 148.8, 145.8, 133.9, 130.8, 118.5, 104.5, 103.0, 93.8, 64.5, 56.2 (2C), 40.7, 36.5, 31.9, 24.1. Anal. ($\text{C}_{16}\text{H}_{22}\text{N}_2\text{O}_4$) C, H, N.

5,6-Dimethoxy-1-methyl-1H-indole-2-carboxylic Acid (3-Formylpropyl)amide (12e). To a solution of IBX (371 mg, 1.37 mmol) in DMSO (1.85 mL) was added **11e** (200 mg, 0.684 mmol), and the solution was stirred for 2 h at room temperature under nitrogen. The solution was diluted with water and extracted with ethyl acetate. The combined organic layers were washed with saturated aqueous NaHCO_3 , water, dried over Na_2SO_4 , and evaporated. The crude product was crystallized from ethyl acetate to give 120 mg (61%) of **12e**, mp 102 °C. ^1H NMR (acetone- d_6) δ : 9.81 (t, J = 1.5 Hz, 1H), 7.77–7.60 (br s, 1H), 7.05 (s, 1H), 7.02 (s, 1H), 6.91 (s, 1H), 4.03 (s, 3H), 3.91 (s, 3H), 3.80 (s, 3H), 3.70 (q, J = 6.7 Hz, 2H), 2.77 (td, J = 6.7 Hz, J = 1.5 Hz, 2H). ^{13}C NMR (75 MHz, acetone- d_6) δ : 201.1, 162.3, 153.8, 149.4, 146.2, 134.2, 118.8, 103.9, 102.9, 93.1, 55.5, 53.3, 43.7, 33.0, 31.0. Anal. ($\text{C}_{15}\text{H}_{18}\text{N}_2\text{O}_4$) C, H, N.

5,6-Dimethoxy-1-methyl-1H-indole-2-carboxylic Acid (3-Oxobutyl)amide (12f). Compound **11f** (178 mg, 0.58 mmol) was suspended in ethyl acetate (19.7 mL), and IBX (473 mg, 1.74 mmol) was added. The resulting mixture was refluxed for 3 h, and then the reaction was cooled to room temperature and filtered. The solid was washed with ethyl acetate and the combined filtrates were concentrated to yield 150 mg (85%) of **12f**, mp 135–136 °C. ^1H NMR (DMSO- d_6) δ : 8.27 (t, J = 5.9 Hz, 1H), 7.07 (s, 1H), 7.03 (s, 1H), 6.92 (s, 1H), 3.93 (s, 3H), 3.83 (s, 3H), 3.76 (s, 3H), 3.46–3–38 (m, 2H), 2.72 (t, J = 7.1 Hz, 2H), 2.13 (s, 3H). ^{13}C NMR (75 MHz, DMSO- d_6) δ : 207.9, 162.3, 146.9, 145.8, 134.9, 133.9, 131.5, 130.5, 118.5, 104.7, 103.0, 93.8, 56.2, 56.1, 43.1, 34.6, 32.0, 30.3. Anal. ($\text{C}_{16}\text{H}_{20}\text{N}_2\text{O}_4$) C, H, N.

5,6-Dimethoxy-1-methyl-1H-indole-2-carboxylic Acid [3-(4-Methoxyphenyl)-3-oxopropyl]amide (12g). To a suspension of **4b** (47.5 mg, 0.20 mmol) in dry THF (1.09 mL) were added EDC (59.3 mg, 0.30 mmol) and HOBt (40.9 mg, 0.30 mmol). The mixture was stirred at room temperature, under nitrogen, for 3 h. 3-Amino-1-(4-methoxyphenyl)propan-1-one trifluoromethanesulfonate (133 mg, 0.404 mmol) was added followed by *N*-ethyl-diisopropylamine (69 μL , 0.4 mmol). After the mixture was stirred for 1 h at room temperature, the solvent was evaporated and the crude product was poured into saturated NaHCO_3 and extracted with ethyl acetate. The combined extracts were then washed with 1 N HCl, saturated aqueous NaHCO_3 , dried over Na_2SO_4 , and concentrated. The crude product was purified by flash chromatography (ethyl acetate/hexane 60:40) to give 45 mg (56%) of **12g**, mp 136 °C. ^1H NMR (DMSO- d_6) δ : 8.35 (t, J = 5.6 Hz, 1H), 7.98 (d, J = 8.9 Hz, 2H), 7.07 (s, 1H), 7.05 (d, J = 8.9 Hz, 2H), 7.02 (s, 1H), 6.92 (s, 1H), 3.93 (s, 3H), 3.83 (s, 6H), 3.75 (s, 3H), 3.55 (dt, J = 7.07 Hz, J = 5.6 Hz, 2H), 3.26 (t, J = 7.1 Hz, 2H). Anal. ($\text{C}_{22}\text{H}_{24}\text{N}_2\text{O}_5$) C, H, N.

7,8-Dimethoxy-10-methyl-3,10-dihydro-2H-azepino[3,4-*b*]indol-1-one (1e). (A) Trifluoroacetic acid (19.7 μL , 0.26 mmol) was added to a solution of **12e** (50 mg, 0.172 mmol) in CH_3CN (3.16 mL), and the mixture was refluxed for 1 h. The solvent was evaporated and the crude product was purified by preparative layer chromatography (ethyl acetate/hexane 95:5) to give 22 mg (47%) of **1e**, mp 208 °C. ^1H NMR (DMSO- d_6) δ : 7.80 (t, J = 5.6 Hz, 1H), 7.26 (s, 1H), 7.14 (d, J = 9.7 Hz, 1H), 7.07 (s, 1H), 6.13–6.00 (m, 1H), 3.97 (s, 3H), 3.88 (s, 3H), 3.80 (s, 3H), 3.5–3.4 (m, 2H). ^{13}C NMR (75 MHz, DMSO- d_6) δ : 163.4, 149.3, 146.1, 133.7, 129.7, 125.7, 117.5, 117.2, 101.7, 101.5, 93.4, 56.4 (2C), 39.9 (one peak missing due to overlapping with solvent signal), 32.8. Anal. ($\text{C}_{15}\text{H}_{16}\text{N}_2\text{O}_3$) C, H, N. (B) InCl_3 (15 mg, 0.068 mmol) was added to **12e** (40 mg, 0.14 mmol) in CH_3CN (2.4 mL), and the mixture was refluxed for 2 h. Evaporation and PLC (ethyl acetate/hexane 95:5) gave 12 mg (32%) of **1e**.

7,8-Dimethoxy-5,10-dimethyl-3,10-dihydro-2H-azepino[3,4-*b*]indol-1-one (1f). Trifluoroacetic acid (121 μL , 1.57 mmol) was added to a solution of **12f** (60 mg, 0.197 mmol) in CH_3CN (3.62 mL), and the mixture was refluxed for 18 h. The solvent was removed, and the crude product was poured into saturated aqueous NaHCO_3 and extracted with ethyl acetate. The organic phase was dried over Na_2SO_4 and filtered and the solvent was evaporated to give 27 mg (47%) of **1f** after crystallization from acetone, mp 238 °C. ^1H NMR (DMSO- d_6) δ : 8.06 (t, J = 5.6 Hz, 1H), 7.26 (s, 1H), 7.10 (s, 1H), 5.80 (t, J = 6.7 Hz, 1H), 3.94 (s, 3H), 3.89 (s, 3H), 3.81 (s, 3H), 3.35–3.20 (m, 2H), 2.37 (s, 3H). ^{13}C NMR (75 MHz, DMSO- d_6) δ : 168.1, 154.1, 150.3, 140.3, 138.6, 135.1, 127.4, 123.6, 121.6, 108.8, 96.5, 61.1, 60.9, 42.7, 37.1, 25.9. Anal. ($\text{C}_{16}\text{H}_{18}\text{N}_2\text{O}_3$) C, H, N.

7,8-Dimethoxy-5-(4-methoxyphenyl)-10-methyl-3,10-dihydro-2H-azepino[3,4-*b*]indol-1-one (1g). Trifluoroacetic acid (80 μL , 1.04 mmol) was added to a suspension of **12g** (42 mg, 0.106 mmol) in CH_3CN (1 mL), and the mixture was refluxed for 18 h. The solvent was evaporated, and the residue was poured into saturated aqueous NaHCO_3 and extracted with ethyl acetate. The combined organic layers were dried over Na_2SO_4 and filtered, and the solvent was evaporated in vacuo. The crude product was purified by PLC (dichloromethane/methanol 97:3) to give 18 mg (43%) of **1g**, mp 198 °C. ^1H NMR (acetone- d_6) δ : 7.26 (t, J = 6.5 Hz, 1H), 7.25 (d, J = 8.7 Hz, 1H), 7.05 (s, 1H), 6.92 (d, J = 8.7 Hz, 2H), 6.10 (t, J = 6.5 Hz, 1H), 6.02 (s, 1H), 4.03 (s, 3H), 3.90 (s, 3H), 3.83 (s, 3H), 3.60 (t, J = 6.51 Hz, 2H), 3.35 (s, 3H). ^{13}C NMR (75 MHz, acetone- d_6) δ : 163.4, 159.6, 149.6, 145.3, 140.8, 133.8, 133.3, 131.0, 129.6 (2C), 121.9, 117.3, 117.0, 113.5 (2C), 104.4, 92.9, 55.3, 54.7, 38.1, 31.3.

Cell Culture and Antibodies. Cells were maintained in Dulbecco's modified Eagle medium supplemented with 5% serum for NIH3T3^{MEN2A} or 10% calf serum (Colorado Serum Company, Denver, CO) for NIH3T3 and NIH3T3^{H-Ras} and incubated at 37 °C in a 10% CO_2 atmosphere. Antiproliferative activity was evaluated by cell counting after 72 h of treatment with compounds dissolved in DMSO or solvent (0.5% final concentration). IC_{50} values were calculated from dose–response curves. The effect of selected compounds on tyrosine phosphorylation and expression of the RET oncoprotein was assessed by Western blot analysis of NIH3T3^{MEN2A} cells after 24 h of treatment as previously described.¹⁷ The following antibodies were used: monoclonal anti-pTyr antibody clone 4610 (Upstate Biotechnology, Lake Placid, NY), rabbit polyclonal anti-Ret H300 and antiphospho Ret (Y1062) (Santa Cruz Biotechnology, Santa Cruz, CA), and anti-actin (Sigma Chemical Company, St. Louis, MO).

Kinase Assay. A nonradioactive kinase assay was performed using recombinant Ret active protein (Upstate, Lake Placid, NY) and myelin basic protein (MBP) (Sigma) as kinase substrate, as previously described.¹⁹ Briefly, the kinase activity was assayed in the presence of Ret (30 ng), 2 μM MBP, solvent, or inhibitor (DMSO 4% final concentration), and 5 μM ATP. After 10 min of incubation at 30 °C, the enzyme-catalyzed reaction was terminated by addition of 3-fold concentrated Laemmli buffer. Samples were subjected to SDS–PAGE and immunoblotted with antiphosphotyrosine antibody. Phosphorylated MBP was revealed by enhanced chemiluminescence reaction (GE Healthcare, Little Chalfont, U.K.). Signal intensity was detected by ChemiDoc XRS system, PC, and analyzed with the interfaced software Quantity One 4.6.3 (Biorad, Hercules, CA).

Docking Methods. The crystal structure of RET (PDB code 2ivu²⁶) was taken from the Protein Data Bank.³² After addition of hydrogen atoms and correction of the wrong residues, the protein complexed with its reference inhibitor (i.e., ZD6474) was minimized using AMBER 9 software³³ and the parm03 force field at 300 K. The complex was placed in a rectangular parallelepiped water box, an explicit solvent model for water, TIP3P, was used, and the complex was solvated with a 8 Å water cap. Chlorine ions were added as counterions to neutralize the system. Two steps of minimization were then carried out. In the first stage, we kept the complex fixed with a position restraint of 500 (kcal/mol)/Å² and we solely minimized the positions of the water molecules. In the

second stage, we minimized the entire system through 5000 steps of steepest descent followed by conjugate gradient (CG) until a convergence of 0.05 kcal/(Å·mol) was attained.

The ligands were built by means of Maestro³⁴ and were then minimized in a water environment (using the generalized Born/surface-area model) by means of MacroModel.³⁵ They were minimized using the CG method until a convergence value of 0.05 kcal/(Å·mol) was attained, using the MMFFs force field and a distance-dependent dielectric constant of 1.0.

The ligands minimized in this manner were docked into the RET binding site by means of GOLD 3.2.²⁷ The region of interest used by GOLD was defined to contain the atoms that stayed within 10 Å of ZD6474 in the minimized receptor model. The “allow early termination” command was deactivated. All the other parameters were used as GOLD default values, and the ligands were submitted to 30 genetic algorithm runs. The docking analysis was carried out using the ChemScore kinase fitness scoring function, and the best docked conformation was then analyzed.

MD Simulations. All simulations were performed using AMBER 9.³³ MD simulations were carried out using the parm03 force field at 300 K. The complex was placed in a rectangular parallelepiped water box, an explicit solvent model for water, TIP3P, was used, and the complex was solvated with a 8 Å water cap. Chlorine ions were added as counterions to neutralize the system. Prior to MD simulations, two steps of minimization were carried out. In the first stage, we kept the protein fixed with a position restraint of 500 (kcal/mol)/Å², and we solely minimized the positions of the water molecules. In the second stage, we minimized the entire system by applying a constraint of 20 kcal/mol on the α carbon. The two minimization stages consisted of 5000 steps of steepest descent followed by CG until a convergence of 0.05 kcal/(Å·mol) was attained.

MD was done on a 1 CPU/node, 4 node, 1024 MB RAM/node cluster Intel Core 2 Duo E6600, 2.4 GHz, and the average wall clock time for a 1 ns simulation was about 33 h.

Particle mesh Ewald (PME)³⁶ electrostatics and periodic boundary conditions were used in the simulation. The MD trajectory was run using the minimized structure as the starting conformation. The time step of the simulations was 2.0 fs with a cutoff of 10 Å for the nonbonded interaction, and SHAKE was employed to keep all bonds involving hydrogen atoms rigid. Constant-volume periodic boundary MD was carried out for 80 ps, during which the temperature was raised from 0 to 300 K. Then 1 ns of constant-pressure periodic boundary MD was carried out at 300 K using the Langevin thermostat to maintain constant the temperature of our system.

The α carbons of the receptor were blocked with a harmonic force constant of 20 (kcal/mol)/Å² during the simulation. General Amber force field (GAFF) parameters were assigned to the ligands, while partial charges were calculated using the AM1-BCC method as implemented in the Antechamber suite of AMBER 9.

Energy Evaluation. We extracted from the last 800 ps of MD of the **2b**– and **2a**–RET complexes 400 snapshots (at time intervals of 2 ps) for each species (complex, receptor, and ligand). In general, the binding free energy of a protein–ligand complex (ΔG_{bind}) is defined as

$$\Delta G_{\text{bind}} = G_{\text{complex}} - (G_{\text{protein}} + G_{\text{ligand}})$$

where G_{complex} , G_{protein} , and G_{ligand} are the free energies of the complex, protein, and the ligand respectively.

For each system the free energy can be estimated as

$$G = E_{\text{MM}} + G_{\text{sol}} - TS$$

Electrostatic, van der Waals energies, and internal energies (E_{MM}) were obtained using the SANDER module in AMBER 9.0.³³ The solvation free energy (G_{sol}) was obtained from the sum of the polar solvation and nonpolar solvation free energy. The polar energy was obtained using the Sander module, applying dielectric constants of 1 and 80 for the solute and the solvent, respectively. Nonpolar

energies were determined using the MOLSURF program applying the LCPO method.³⁷

Acknowledgment. We are indebted to Cell Therapeutics, Bresso, Italy, for a generous gift of 5,6-dimethoxyindolin-2-one and RPI-1 and to Laura Zanesi for aid in editing the manuscript. This work was partially supported by Associazione Italiana per la Ricerca sul Cancro, Milan, Italy, by Alleanza Contro il Cancro, Italy, and by University of Milano (FIRST funds). Molecular graphics images were produced using the UCSF Chimera package from the Resource for Biocomputing, Visualization, and Informatics at the University of California, San Francisco (supported by NIH Grant P41 RR-01081).

Supporting Information Available: Elemental analysis of analysis data of the compounds. This material is available free of charge via the Internet at <http://pubs.acs.org>.

References

- Arighi, E.; Borrello, M. G.; Saria, H. RET tyrosine kinase signaling in development and cancer. *Cytokine Growth Factor Rev.* **2005**, *16*, 441–467.
- Asai, N.; Jijiwa, M.; Enomoto, A.; Hawai, K.; Maeda, K.; Ichihara, M.; Murakumo, Y.; Takahashi, M. RET receptor signaling: dysfunction in thyroid cancer and Hirschsprung's disease. *Pathol. Int.* **2006**, *56*, 164–172.
- Murakumo, Y.; Jijiwa, M.; Asai, N.; Ichihara, M.; Takahashi, M. RET and neuroendocrine tumors. *Pituitary* **2006**, *9*, 179–192.
- Rosa, D. D.; Ismael, G.; Dal Lago, L.; Awada, A. Molecular-targeted therapies: lessons from years of clinical development. *Cancer Treat. Rev.* **2008**, *34*, 61–80.
- Drosten, M.; Pützer, B. M. Mechanisms of disease: cancer targeting and the impact of oncogenic RET for medullary thyroid carcinoma therapy. *Nat. Clin. Pract.* **2006**, *3*, 564–574.
- De Groot, J. W. B.; Links, T. P.; Plukker, J. T. M.; Lips, C. J. M.; Hofstra, R. M. W. RET as a diagnostic and therapeutic target in sporadic and hereditary endocrine tumors. *Endocr. Rev.* **2006**, *27*, 535–560.
- Cuccuru, G.; Lanzi, C.; Cassinelli, G.; Pratesi, G.; Tortoreto, M.; Petrangolini, G.; Seregni, E.; Martinetti, A.; Laccabue, D.; Zanchi, C.; Zunino, F. Cellular effects and antitumor activity of RET inhibitor RPI-1 on MEN2A-associated medullary thyroid carcinoma. *J. Natl. Cancer Inst.* **2004**, *96*, 1006–1014.
- Drosten, M.; Hilken, G.; Böckmann, M.; Rödicker, F.; Mise, N.; Cranston, A. N.; Dahmen, U.; Ponder, B. A. J.; Pützer, B. M. Role of MEN2A-derived RET in maintenance and proliferation of medullary thyroid carcinoma. *J. Natl. Cancer Inst.* **2004**, *96*, 1231–1239.
- Petrangolini, G.; Cuccuru, G.; Lanzi, C.; Tortoreto, M.; Belluco, S.; Pratesi, G.; Cassinelli, G.; Zunino, F. Apoptotic cell death induction and angiogenesis inhibition in large established medullary thyroid carcinoma xenografts by Ret inhibitor RPI-1. *Biochem. Pharmacol.* **2006**, *72*, 405–414.
- Sharma, S. V.; Settleman, J. Oncogene addiction: setting the stage for molecularly targeted cancer therapy. *Genes Dev.* **2007**, *21*, 3214–3231.
- Cassinelli, G.; Lanzi, C.; Pensa, T.; Gambetta, R. A.; Nasini, G.; Cuccuru, G.; Cassinis, M.; Pratesi, G.; Polizzi, D.; Tortoreto, M.; Zunino, F. Clavilactones, a novel class of tyrosine kinase inhibitors of fungal origin. *Biochem. Pharmacol.* **2000**, *59*, 1539–1547.
- Kundra, P.; Burman, K. D. Thyroid cancer molecular signaling pathways and use of targeted therapy. *Endocrinol. Metab. Clin. N. Am.* **2007**, *36*, 839–853.
- Deshpande, H. A.; Gettinger, S. N.; Sosa, J. A. Novel chemotherapy options for advanced thyroid tumors: small molecules offer great hope. *Curr. Opin. Oncol.* **2008**, *20*, 19–24.
- Schlumberger, M.; Carlomagno, F.; Baudin, E.; Bidart, J. M.; Santoro, M. New therapeutic approaches to treat medullary thyroid carcinoma. *Nat. Clin. Pract.* **2008**, *4*, 22–32.
- Sun, L.; Tran, N.; Tang, F.; App, H.; Hirth, P.; McMahon, G.; Tang, C. Synthesis and biological evaluations of 3-substituted indolin-2-ones: a novel class of tyrosine kinase inhibitors that exhibit selectivity toward particular receptor tyrosine kinases. *J. Med. Chem.* **1998**, *41*, 2588–2603.
- Lanzi, C.; Cassinelli, G.; Cuccuru, G.; Zaffaroni, N.; Supino, R.; Vignati, S.; Zanchi, C.; Yamamoto, M.; Zunino, F. Inactivation of Ret/Ptc1 oncoprotein and inhibition of papillary thyroid carcinoma cell proliferation by indolinone RPI-1. *Cell. Mol. Life Sci.* **2003**, *60*, 1449–1459.

- (17) Lanzi, C.; Cassinelli, G.; Pensa, T.; Cassinis, M.; Gambetta, R. A.; Borrello, M. G.; Menta, E.; Pierotti, M. A.; Zunino, F. Inhibition of transforming activity of the ret/ptc1 oncoprotein by a 2-indolinone derivative. *Int. J. Cancer* **2000**, *85*, 384–390.
- (18) Cassinelli, C.; Lanzi, C.; Petrangolini, G.; Tortoreto, M.; Pratesi, G.; Cuccuru, G.; Laccabue, D.; Supino, R.; Belluco, S.; Favini, E.; Poletti, A.; Zunino, F. Inhibition of c-Met and prevention of spontaneous metastatic spreading by the 2-indolinone RPI-1. *Mol. Cancer Ther.* **2006**, *5*, 2388–2397.
- (19) Sun, L.; Tran, N.; Tang, F.; App, H.; Hirth, P.; McMahon, G.; Tang, C. Synthesis and biological evaluations of 3-substituted indolin-2-ones: a novel class of tyrosine kinase inhibitors that exhibit selectivity toward particular receptor tyrosine kinases. *J. Med. Chem.* **1998**, *41*, 2588–2603.
- (20) Tuccinardi, T.; Manetti, F.; Schenone, S.; Martinelli, A.; Botta, M. Construction and validation of a RET TK catalytic domain by homology modeling. *J. Chem. Inf. Model.* **2007**, *47*, 644–655.
- (21) Mohammadi, M.; McMahon, G.; Sun, L.; Tang, C.; Hirth, P.; Yeh, B. K.; Hubbard, S. R.; Schlessinger, J. Structures of the tyrosine kinase domain of fibroblast growth factor receptor in complex with inhibitors. *Science* **1997**, *276*, 955–960.
- (22) Wang, S.; Dong, Y.; Wang, X.; Hu, X.; Liu, J. O.; Hu, Y. 3-Aryl beta-carbolin-1-ones as a new class of potent inhibitors of tumor cell proliferation: synthesis and biological evaluation. *Org. Biomol. Chem.* **2005**, *3*, 911–916.
- (23) Chacun-Lefèvre, B.; Joseph, B.; Méroux, J.-Y. Synthesis and reactivity of azepino[3,4-*b*]indol-5-yl trifluoromethanesulfonate. *Tetrahedron* **2000**, *56*, 4491–4499.
- (24) Cincinelli, R.; Dallavalle, S.; Merlini, L. Intramolecular Friedel–Crafts reaction of indoles with carbonyl groups: a simple synthesis of 3- and 4-substituted β -carbolin-1-ones. *Synlett* **2008**, 1309–1312.
- (25) Rizzi, E.; Cassinelli, G.; Dallavalle, S.; Lanzi, C.; Cincinelli, R.; Nannei, R.; Cuccuru, G.; Zunino, F. Synthesis and RET protein kinase inhibitory activity of 3-aryleidobenzylidene-indolin-2-ones. *Bioorg. Med. Chem. Lett.* **2007**, *17*, 3962–3968.
- (26) Knowles, P. P.; Murray-Rust, J.; Kjaer, S.; Scott, R. P.; Hanrahan, S.; Santoro, M.; Ibáñez, C. F.; McDonald, N. Q. Structure and chemical inhibition of the RET tyrosine kinase domain. *J. Biol. Chem.* **2006**, *281*, 33577–33587.
- (27) Jones, G.; Willett, P.; Glen, R. C.; Leach, A. R.; Taylor, R. Development and validation of a genetic algorithm for flexible docking. *J. Mol. Biol.* **1997**, *267*, 727–748.
- (28) Toledo, L. M.; Lydon, N. B.; Elbaum, D. The structure-based design of ATP-site directed protein kinase inhibitors. *Curr. Med. Chem.* **1999**, *6*, 775.
- (29) Traxler, P.; Green, J.; Mett, H.; Sequin, U.; Furet, P. Use of a pharmacophore model for the design of EGFR tyrosine kinase inhibitors: isoflavones and 3-phenyl-4(1*H*)-quinolones. *J. Med. Chem.* **1999**, *42*, 1018–1026.
- (30) Massova, I.; Kollman, P. A. Combined molecular mechanical and continuum solvent approach (MM-PBSA/GBSA) to predict ligand binding. *Perspect. Drug Discovery Des.* **2000**, *18*, 113–135.
- (31) Rizzo, R. C.; Toba, S.; Kuntz, I. D. A molecular basis for the selectivity of thiazazole urea inhibitors with stromelysin-1 and gelatinase-A from generalized Born molecular dynamics simulations. *J. Med. Chem.* **2004**, *47*, 3065–3074.
- (32) <http://www.pdb.org/>.
- (33) Case, D. A.; Darden, T. A.; Cheatham, T. E., III; Simmerling, C. L.; Wang, J.; Duke, R. E.; Luo, R.; Merz, K. M.; Pearlman, D. A.; Crowley, M.; Walker, R. C.; Zhang, W.; Wang, B.; Hayik, S.; Roitberg, A.; Seabra, G.; Wong, K. F.; Paesani, F.; Wu, X.; Brozell, S.; Tsui, V.; Gohlke, H.; Yang, L.; Tan, C.; Mongan, J.; Hornak, V.; Cui, G.; Beroza, P.; Matthews, D. H.; Schafmeister, C.; Ross, W. S.; Kollman, P. A. *AMBER 9*; University of California: San Francisco, CA, 2006.
- (34) *Maestro*, version 7.5; Schrödinger, Inc.: Portland, OR, 1999.
- (35) *Macromodel*, version 8.5; Schrödinger, Inc.: Portland, OR, 1999.
- (36) Essman, U.; Perela, L.; Berkowitz, M. L.; Darden, T.; Lee, H.; Pedersen, L. G. A smooth particle mesh Ewald method. *J. Chem. Phys.* **1995**, *103*, 8577–8592.
- (37) Weiser, J.; Shenkin, P. S.; Still, W. C. Approximate atomic surfaces from linear combinations of pairwise overlaps (LCPO). *J. Comput. Chem.* **1999**, *20*, 217–230.

JM8007823